European Journal of Medicinal Chemistry 63 (2013) 501–510

Contents lists available at SciVerse ScienceDirect

European Journal of Medicinal Chemistry

journal homepage: http://www.elsevier.com/locate/ejmech

Original article

Cytotoxic 3,4,5-trimethoxychalcones as mitotic arresters and cell migration inhibitors

Lívia B. Salum [a], Wanessa F. Altei [a], Louise D. Chiaradia [b], Marlon N.S. Cordeiro [b], Rafael R. Canevarolo [d], Carolina P.S. Melo [d], Evelyn Winter [c], Bruno Mattei [c], Hikmat N. Daghestani [e], Maria Cláudia Santos-Silva [f], Tânia B. Creczynski-Pasa [c], Rosendo A. Yunes [b], José A. Yunes [d], Adriano D. Andricopulo [a], Billy W. Day [g], Ricardo J. Nunes [b,**], Andreas Vogt [h,i,*]

[a] Laboratório de Química Medicinal e Computacional, IFSC – USP, São Carlos, SP, Brazil
[b] Laboratório Estrutura e Atividade, Departamento de Química, UFSC, Florianópolis, SC, Brazil
[c] Departamento de Ciências Farmacêuticas, UFSC, Florianópolis, SC, Brazil
[d] Centro Infantil Boldrini, Campinas, SP, Brazil
[e] Department of Structural Biology, University of Pittsburgh, Pittsburgh, PA 15260, USA
[f] Departamento de Análises Clínicas, UFSC, Florianópolis, SC, Brazil
[g] Department of Pharmaceutical Sciences, University of Pittsburgh, Pittsburgh, PA 15260, USA
[h] Department of Computational and Systems Biology, University of Pittsburgh, Pittsburgh, PA 15260, USA
[i] University of Pittsburgh Drug Discovery Institute, University of Pittsburgh, Pittsburgh, PA 15260, USA

ARTICLE INFO

Article history:
Received 22 November 2012
Received in revised form
22 February 2013
Accepted 25 February 2013
Available online 6 March 2013

Keywords:
Chalcones
Microtubule perturbing agents
High-content screening
Mitotic index

ABSTRACT

Based on classical colchicine site ligands and a computational model of the colchicine binding site on beta tubulin, two classes of chalcone derivatives were designed, synthesized and evaluated for inhibition of tubulin assembly and toxicity in human cancer cell lines. Docking studies suggested that the chalcone scaffold could fit the colchicine site on tubulin in an orientation similar to that of the natural product. In particular, a 3,4,5-trimethoxyphenyl ring adjacent to the carbonyl group appeared to benefit the ligand –tubulin interaction, occupying the same subcavity as the corresponding moiety in colchicine. Consistent with modeling predictions, several 3,4,5-trimethoxychalcones showed improved cytotoxicity to murine acute lymphoblastic leukemia cells compared with a previously described parent compound, and inhibited tubulin assembly *in vitro* as potently as colchicine. The most potent chalcones inhibited the growth of human leukemia cell lines at nanomolar concentrations, caused microtubule destabilization and mitotic arrest in human cervical cancer cells, and inhibited human breast cancer cell migration in scratch wound and Boyden chamber assays.

1. Introduction

Microtubules (MTs) are cytoskeletal polymers of α and β tubulin heterodimers involved in several critical cellular functions, including motility, division and intracellular transport. Interference with either assembly or disassembly of MTs in dividing cells provokes cell cycle arrest, triggering signals that induce apoptosis. Therefore, the design of MT perturbing agents is one of the current front-line approaches to anticancer therapy [1].

MT-targeting agents usually bind to one of three major binding sites on tubulin, named taxane, vinca and colchicine sites. While taxanes and vinca alkaloids have tremendously impacted the treatment of human cancers, the high toxicity of colchicine (**1a**) and podophyllotoxin (**1b**) (Fig. 1) has limited their therapeutic

Abbreviations: Cy3, indocarbocyanine dye with three-methine linker; DMEM, Dulbecco's Modified Eagle's Medium; DMSO, dimethyl sulfoxide; FITC, fluorescein isothiocyanate; HBSS, Hank's balanced salt solution; HCS, high-content screening; HUVEC, human umbilical vein endothelial cells; MDEC, minimal detectable effective concentration; MT, microtubules; MTT, 3-(4,5-dimethylthiazol-2-yl)-2,5-diphenyltetrazolium bromide; PBMC, peripheral blood mononuclear cells; RPMI, Roswell Park Memorial Institute medium.

* Corresponding author. Department of Computational and Systems Biology, 10047 Biomedical Science Tower 3, 3501 Fifth Avenue, University of Pittsburgh, Pittsburgh, PA 15260, USA. Tel.: +1 412 383 5856; fax: +1 412 648 9009.
** Corresponding author. Laboratório Estrutura e Atividade, Departamento de Química, Universidade Federal de Santa Catarina, Campus Trindade, CEP 88040-900 Florianópolis, SC, Brazil. Tel.: +55 48 3721 6844x236.
E-mail addresses: ricardo.nunes@ufsc.br (R.J. Nunes), avogt@pitt.edu (A. Vogt).

0223-5234/$ – see front matter © 2013 Elsevier Masson SAS. All rights reserved.
http://dx.doi.org/10.1016/j.ejmech.2013.02.037

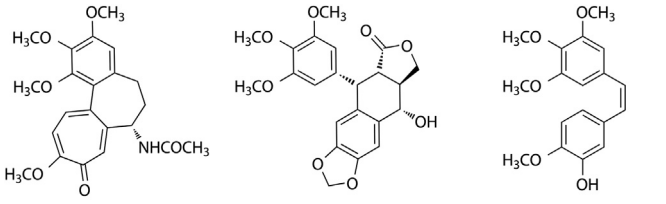

Fig. 1. Representative microtubule-interacting agents that bind to the colchicine site on tubulin.

application for the therapy of cancer. Because the utility of clinically used MT perturbing agents is compromised by drug resistance, adverse side effects, complex formulations, synthetic complexity, scarceness and limited bioavailability, the search for novel, structurally simpler small molecule modulators of the tubulin/MT system has been a priority for many years [1–3]. Lately, the biological properties of the colchicine site ligand combretastatin A-4 (**1c**) (Fig. 1), a potent inhibitor of tubulin assembly and cell growth that also has antiangiogenic activity [4,5] have renewed interest in the development of colchicine analogs as potential anticancer agents. Moreover, the fact that combretastatin A-4 is not recognized by P-glycoprotein, which is related to multidrug resistance, has reinforced the significance of colchicine site ligands as antitubulin agents [4,5]. In this context, the chemically versatile and easily synthesized chemical class of chalcones **2** (Fig. 2) represents an attractive scaffold for the design of novel colchicine site ligands that inhibit tubulin assembly. In fact, several studies have demonstrated that chalcone derivatives are cytotoxic against a variety of cell lines and may have potential applications in cancer treatment (reviewed in Ref. [6]).

Although antimitotic chalcones have been identified in the 1980's (reviewed in Ref. [7]), considerable efforts are being dedicated to identify new chalcone-based leads within the oncology field, due to their anticancer properties and simple synthesis. The most recent advances include photodynamic agents [8], dihalogenated chalcones [9], and peptidyl [10] and boronic acid derivatives [11]. Work within our own group has led to the development of the chalcone **2b** (Fig. 2), derived from 2-naphtaldehyde, that was selectively cytotoxic to L-1210 murine acute lymphoblastic leukemia cells and promoted cell cycle arrest

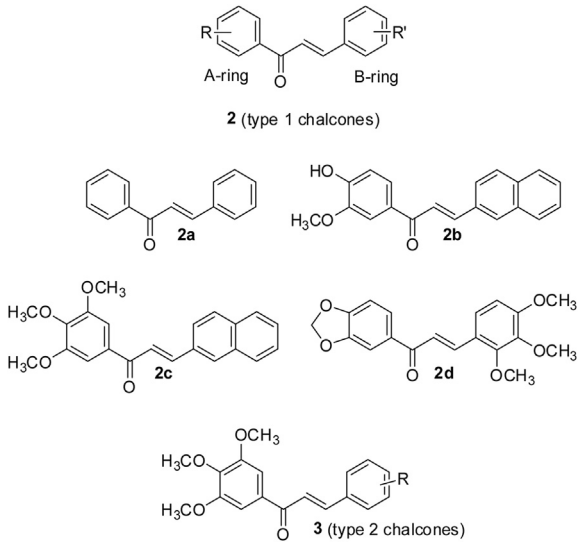

Fig. 2. Type 1 and type 2 chalcones.

and apoptosis [12]. As part of our ongoing efforts to design improved inhibitors of tubulin polymerization, we synthesized a series of type 1 chalcones (**2a**–**2d**) (Fig. 2) with aromatic substitution patterns mimicking those in classical colchicine site ligands (Fig. 1). Consistent with molecular modeling predictions, the trimethoxy derivative **2c** was more potent than the parent compound (**2b**) in L-1210 proliferation and tubulin assembly inhibition assays, motivating the synthesis and assessment of a novel series of 3,4,5-trimethoxychalcones (type 2 chalcones) **3** (Fig. 2). In the new series, the majority of analogs retained growth inhibitory activity against L-1210 cells (Supplemental Table S1). The most potent type 1 and type 2 chalcones were further evaluated for cytotoxicity in REH and Jurkat human leukemia cells, for mitotic arrest and alterations in cellular MT morphology using high-content analysis in human cervical cancer cells, and for antimigratory activity in human breast cancer cells using scratch wounding and Boyden chamber cell migration assays. The most active analogs, **2c** and **3a,** inhibited tubulin assembly *in vitro* as potently as colchicine and showed submicromolar activity in the human cancer cell assays.

2. Material and methods

2.1. Synthesis

2.1.1. Preparation of compounds

Reagents used were obtained commercially from Sigma–Aldrich. Type 1 and 2 chalcones were prepared by aldol condensation of acetophenones (1 mmol) with aldehydes (1 mmol), in methanol (15 mL), KOH (50% v/v), at room temperature with magnetic agitation for 24 h. The volume of KOH varied according to the different inductive and mesomeric effects for the various substituents of the aromatic rings: 2 mL for compounds **2a**, **2b** and **2c**; 40 drops for compounds **2d** and **3p**; 15 drops for compounds **3d** and **3q**; 13 drops for compounds **3a**, **3h**, **3j** and **3o**; 10 drops for compounds **3b**, **3c**, **3e**, **3f**, **3i** and **3k**; 8 drops for compounds **3n**, **3r** and **3s**; and 5 drops for compounds **3g**, **3l** and **3m**. KOH addition was stopped at the first sign of precipitation. Distilled water and 10% hydrochloric acid were added to the reaction for total precipitation of the compounds, which were then obtained by vacuum filtration and later recrystallized in dichloromethane, with forced precipitation by hexane. The purity of the synthesized compounds was analyzed by thin-layer chromatography (TLC) using Merck silica pre-coated aluminum plates of 200 μm thickness, with several solvent systems of different polarities. Compounds were visualized with ultraviolet light (λ = 254 and 360 nm) and using sulfuric anisaldehyde solution followed by heat application as the developing agent. The chalcones were soluble in dimethyl sulfoxide, acetone, acetyl acetate, chloroform and dichloromethane. Compounds **3a**–**3o** and **3r** were previously cited in the literature [6,7,16–21]. Chalcone derivatives **2a**, **2b** and **2c** were previously synthesized by our group [13–15] and **2d**, **3p**, **3q** and **3s** are novel compounds.

2.1.2. Physico–chemical data of the compounds

The structures were confirmed by melting points (m.p.), infrared spectroscopy (IR) and ^{1}H and ^{13}C nuclear magnetic resonance spectroscopy (NMR), as well as elementary analysis for previously undescribed structures. Melting points were determined with a Microquímica MGAPF-301 apparatus and are uncorrected. IR spectra were recorded with an Abb Bomen FTLA 2000 spectrometer on KBr disks. Elementary analysis was carried out using a CHNS EA 1110; percentages of C and H were in agreement with the product formula (within ±0.4% of theoretical values for C). NMR (^{1}H and ^{13}C) spectra were recorded on a Varian Oxford AS-400 (400 MHz) instrument, using tetramethylsilane as an internal standard. ^{1}H

NMR spectra revealed that structures were geometrically pure and configured *E* ($J_{H\alpha-H\beta} = \sim 16$ Hz), except **3a**, which is a mixture of *E* ($J_{H\alpha-H\beta} = 16$ Hz) 2:1 *Z* ($J_{H\alpha-H\beta} = 12$ Hz) isomers.

2.1.2.1. ***2c*** *– (2E)-1-(3′,4′,5′-trimethoxyphenyl)-3-(2-naphthyl)-2-propen-1-one.* Light yellow solid, m.p. 131–132 °C; ^{1}H NMR ($CDCl_3$) δ 3.96 (s, 6H, OCH_3), 3.98 (s, 3H, OCH_3), 7.32 (s, 2H, H2′, H6′), 7.54 (m, 2H, H3, H6), 7.60 (d, 1H, J = 15.6 Hz, Hα), 7.83 (d, 1H, J = 8.0 Hz, H7), 7.87 (m, 2H, H5, H8), 7.89 (m, 1H, H4), 7.99 (d, 1H, J = 15.6 Hz, Hβ), 8.05 (s, 1H, H1). ^{13}C NMR ($CDCl_3$) δ 56.66 (*m*-OCH_3), 61.28 (*p*-OCH_3), 106.29 (C2′, C6′), 122.04 (C3), 123.86 (Cα), 127.07 (C1), 127.68 (C6), 128.07 (C7), 128.90 (C5), 128.98 (C8), 130.99 (C4), 132.59 (C1′), 133.59 (C2), 133.84 (C4a), 134.61 (C8a), 145.14 (C4′, Cβ), 153.40 (C3′, C5′), 189.47 (C=O). IR ν_{max}/cm^{-1} 1656 (C=O), 1582 (C=C), 1230 (C–O), 2834, 1502, 1458, 1411, 996, 813 (Ar) (KBr). Anal. Calcd for $C_{22}H_{20}O_4$: C 75.84, H 5.79. Found: C 75.53, H 5.81. Yield = 97%.

2.1.2.2. ***2d*** *– (2E)-1-(1′,3′-benzodioxol-5-yl)-3-(2,3,4-trimethoxyphenyl)-2-propen-1-one.* Light yellow solid, m.p. 100–101 °C; ^{1}H NMR ($CDCl_3$) δ 3.89 (s, 3H, OCH_3), 3.90 (s, 3H, OCH_3), 3.94 (s, 3H, OCH_3), 6.05 (s, 2H, $-OCH_2O-$), 6.71 (d, 1H, J = 8.0 Hz, H5), 6.88 (d, 1H, J = 8.0 Hz, H5′), 7.36 (d, 1H, J = 8.0 Hz, H6), 7.51 (d, 1H, J = 16.0 Hz, Hα), 7.53 (s, 1H, H2′), 7.64 (dd, 1H, J = 8.0/1.0 Hz, H6′), 7.97 (d, 1H, J = 16.0 Hz, Hβ). ^{13}C NMR ($CDCl_3$) δ 56.07 (OCH_3), 60.92 (OCH_3), 61.39 (OCH_3), 101.78 ($-OCH_2O-$), 107.56 (C5), 107.84 (C2′), 108.45 (C5′), 121.00 (C6), 122.09 (C1), 123.88 (C6′), 124.49 (Cα), 133.32 (C1′), 139.58 (Cβ), 142.48 (C3), 148.19 (C3′), 151.45 (C2), 153.75 (C4′), 156.67 (C4), 188.65 (C=O). IR ν_{max}/cm^{-1} 1652 (C=O), 1583 (C=C), 1249, 1041 (C–O), 3079, 2976, 2942, 2901, 2837, 1492, 1484, 1464, 1446, 1413, 1329, 1301, 1282, 1115, 1095, 988, 942, 916, 815, 697, 506 (Ar) (KBr). Anal. Calcd for $C_{19}H_{18}O_6$: C 66.66, H 5.30. Found: C 66.91, H 5.27. Yield: 94%.

2.1.2.3. ***3a*** *– (2E,Z)-1-(3′,4′,5′-trimethoxyphenyl)-3-(4-dimethylaminophenyl)-2-propen-1-one.* Golden yellow solid, m.p. 148–149 °C; ^{1}H NMR ($CDCl_3$) δ 2.98 (s, 3H, *Z*-CH_3), 3.06 (s, 3H, *E*-CH_3), 3.88 (s, 6H, *Z*-*m*-OCH_3), 33.90 (s, 3H, *Z*-*p*-OCH_3), 3.93 (s, 3H, *E*-*p*-OCH_3), 3.95 (s, 6H, *E*-*m*-OCH_3), 6.44 (d, 1H, J = 12.0 Hz, *Z*-Hα), 6.58 (d, 1H, J = 8.0 Hz, *Z*-H3, *Z*-H5), 6.71 (d, 1H, J = 8.0 Hz, *E*-H3, *E*-H5), 6.90 (d, 1H, J = 12.0 Hz, *Z*-Hβ), 7.19 (2, 2H, *Z*-H2′, *Z*-H6′), 7.27 (2, 2H, *E*-H2′, *E*-H6′), 7.32 (d, 1H, J = 16.0 Hz, *E*-Hα), 7.56 (m, 2H, *E*-H2, *E*-H6), 7.5e (m, 2H, *Z*-H2, *Z*-H6), 7.80 (d, 1H, J = 16.0 Hz, *E*-Hβ). ^{13}C NMR ($CDCl_3$) δ 40.36 (CH_3), 56.57 (*m*-OCH_3), 60.80 (*p*-OCH_3), 106.06 (C2′, C6′), 112.04 (C3, C5), 116.77 (C1), 122.84 (Cα), 130.66 (C2, C6), 134.71 (C1′), 146.04 (Cβ), 141.20 (C4′), 152.29 (C4), 153.27 (C3′, C5′), 189.70 (C=O); in the RMN ^{13}C was possible observe only the *E*-isomer. IR ν_{max}/cm^{-1} 1650 (C=O), 1563 (C=C), 1228, 1006 (C–O), 1153 (C–N), 2942, 2845, 1613, 1549, 1524, 1506, 1432, 1413, 1377, 1347, 1302, 1191, 1126, 1073, 984, 817, 669 (Ar) (KBr). Anal. Calcd for $C_{20}H_{23}NO_4$: C 70.36, H 6.79, N 4.10. Found: C 70.05, H 6.83, N 4.08. Yield: 45%.

2.1.2.4. ***3p*** *– (2E)-1-(3′,4′,5′-trimethoxyphenyl)-3-(5-methylfuran-2-yl)-2-propen-1-one.* Dark yellow solid, m.p. 89–90 °C; ^{1}H NMR ($CDCl_3$) δ 2.41 (s, 3H, CH_3), 3.94 (s, 3H, *p*-OCH_3), 3.95 (s, 6H, *m*-OCH_3), 6.14 (d, 1H, J = 4.0 Hz, H4), 6.44 (d, 1H, J = 4.0 Hz, H5), 7.29 (2, 2H, H2′, H6′), 7.32 (d, 1H, J = 16.0 Hz, Hα), 7.55 (d, 1H, J = 16.0 Hz, Hβ). ^{13}C NMR ($CDCl_3$) δ 14.30 (CH_3), 56.66 (*m*-OCH_3), 61.17 (*p*-OCH_3), 106.17 (C2′, C6′), 109.64 (C4), 117.23 (C5), 118.67 (Cα), 131.07 (Cβ), 133.96 (C1′), 142.48 (C4′), 150.65 (C1), 153.32 (C3′, C5′), 156.20 (C3), 188.85 (C=O). IR ν_{max}/cm^{-1} 1653 (C=O), 1565 (C=C), 1227, 1012 (C–O), 2941, 2839, 1606, 1582, 1503, 1414, 1335, 1158, 1126, 796, 698, 625 (Ar) (KBr). Anal. Calcd for $C_{17}H_{18}O_5$: C 67.54, H 6.00. Found: C 67.76, H 6.42. Yield: 78%.

2.1.2.5. ***3q*** *– (2E)-1-(3′,4′,5′-trimethoxyphenyl)-3-(3-trifluoromethyl-4-chlorophenyl)-2-propen-1-one.* Light yellow solid, m.p. 146–147 °C; ^{1}H NMR ($CDCl_3$) δ 3.95 (s, 3H, *p*-OCH_3), 3.95 (s, 6H, *m*-OCH_3), 7.26 (2, 2H, H2′, H6′), 7.32 (dd, 1H, J = 8.0/1.0 Hz, H5), 7.38 (d, 1H, J = 16.0 Hz, Hα), 7.48 (s, 1H, H2), 7.68 (d, 1H, J = 8.0 Hz, H6), 8.08 (d, 1H, J = 16.0 Hz, Hβ). ^{13}C NMR ($CDCl_3$) δ 56.61 (*m*-OCH_3), 61.16 (*p*-OCH_3), 106.49 (C2′, C6′), 125.32 (Cα), 127.80 (C2), 128.78 (C5), 130.34 (C3), 130.38 (C6), 132.13 (C4), 133.17 (C1′), 136.19 (CF_3), 136.70 (C1), 139.53 (Cβ), 141.59 (C4′), 153.41 (C3′, C5′), 189.40 (C=O). IR ν_{max}/cm^{-1} 1658 (C=O), 1574 (C=C), 1230, 1001 (C–O), 1161 (C–F), 1125 (C–Cl), 3080, 2938, 2838, 1598, 1505, 1451, 1413, 1343, 1314, 1104, 816, 648 (Ar) (KBr). Anal. Calcd for $C_{19}H_{16}ClF_3O_4$: C 56.94, H 4.02. Found: C 57.20, H 4.16. Yield: 90%.

2.1.2.6. ***3s*** *– (2E)-1-(3′,4′,5′-trimethoxyphenyl)-3-(3,5-dichlorophenyl)-2-propen-1-one.* Cream solid, m.p. 136–138 °C; ^{1}H NMR ($CDCl_3$) δ 3.95 (s, 3H, OCH_3), 3.96 (s, 6H, OCH_3), 7.27 (2, 2H, H2′, H6′), 7.40 (m, 1H, H4), 7.46 (d, 1H, J = 16.0 Hz, Hα), 7.50–7.51 (s, 2H, H2, H6), 7.66 (d, 1H, J = 16.0 Hz, Hβ). ^{13}C NMR ($CDCl_3$) δ 56.74 (*m*-OCH_3), 61.74 (*p*-OCH_3), 106.44 (C2′, C6′), 123.85 (Cα), 127.29 (C4), 132.38 (C1′, C2, C6), 133.16 (C3, C5), 134.10 (C1), 141.79 (Cβ), 143.16 (C4′), 153.47 (C3′, C5′), 188.66 (C=O). IR ν_{max}/cm^{-1} 1664 (C=O), 1584 (C=C), 1230, 1003 (C–O), 1132 (C–Cl), 3069, 2945, 2831, 1610, 1564, 1508, 1467, 1418, 1340, 1164, 973, 838, 803, 660 (Ar) (KBr). Anal. Calcd for $C_{18}H_{16}Cl_2O_4$: C 58.87, H 4.39. Found: C 58.61, H 5.00. Yield: 92%.

2.2. Antiproliferative assays

2.2.1. L-1210 mouse leukemia cell assays

2.2.1.1. Cell culture. Murine lymphoblastic leukemia (L1210) cells were obtained from American Type Culture Cell (ATCC). The cells were cultured in RPMI (Roswell Park Memorial Institute medium) supplemented with 10% heat-inactivated fetal bovine serum (FBS), 100 U/mL penicillin, 100 μg/mL streptomycin and 10 mM HEPES. The cell culture was maintained at 37 °C in a 5% CO_2 humidified atmosphere and pH 7.4. Every 2–3 days, cells were passaged by removing 90% of the supernatant and replacing it with fresh medium. In all experiments, viable cells were checked in the beginning of the experiment by the Trypan Blue exclusion test.

2.2.1.2. Cytotoxicity. Cytotoxicity was evaluated with the MTT ((3-(4,5-Dimethylthiazol-2-yl)-2,5-diphenyltetrazolium bromide) assay [37]. 1×10^5 cells/well were incubated for 24 h in triplicate with compounds (solubilized in a maximum of 1% DMSO), at different concentrations (1–100 μM) in 96-well microplates. After incubation at 37 °C, cells were washed with fresh culture medium, and 10 μL of MTT (5 mg/mL) were added followed by incubation at 37 °C for 2 h. The precipitated formazan was dissolved in 100 μL of DMSO, and the absorbance was measured at 540 nm using a micro-well system reader. The IC_{50} values were calculated from a four parameter logistic equation. The chalcones were dissolved in DMSO, and in order to verify if the solvent itself could affect the cells, in all experiments, control curves without chalcones and in the presence of the cells and the solvent were carried out in parallel. The controls with solvent were not statistically different from control cells alone (data not shown).

2.2.2. Cytotoxicity in tumorigenic and non-tumorigenic cell lines

2.2.2.1. Cell culture. REH and JURKAT human acute lymphoblastic leukemia cell lines of precursor B-cell and T-cell immunophenotypes, respectively, were cultured in RPMI-1640 medium supplemented with 10% FBS (RPMI-10), 100 U/mL penicillin and 100 pg/mL streptomycin. Cultures were maintained at 37 °C in a 5% CO_2 humidified atmosphere. NIH3T3 and HUVEC were cultured under the same conditions in RPMI-1640 and DMEM, respectively. Normal

human mononuclear cells were isolated from blood of a healthy individual using Ficoll–Paque (GE Healthcare) gradient, washed twice with PBS buffer and cultured in 96 well plates at 200,000 cell/well in RPMI-10 supplemented with 20 μL/mL of phytohemagglutinin (Cultilab, Campinas, SP, Brazil) and 50 IU/mL of interleukin-2 (Proleukin, ZODIAC) to induce proliferation of T lymphocytes. Cytotoxicity assays were initiated after 24 h of PHA/interleukin-2 stimulation by adding 20 μL of serial chalcone dilutions (see below). For comparison, JURKAT cells (30,000/well) were seeded in the same 96 well plates and cultured for 24 h in RPMI-10 (without PHA or interleukin-2) before treatment.

2.2.2.2. Cytotoxicity assay. For the cytotoxic assay, chalcones were dissolved in DMSO to obtain a stock solution of 20 mM. Further dilutions were made in culture medium (RPMI-10) immediately before use. REH and JURKAT cells were plated at 3×10^4 cells/well in 80 μL RPMI-10. Immediately, 20 μL of 10-fold serial chalcone dilutions were added to each well, in triplicate, at final concentrations of 0.01–100 μM. DMSO used as a vehicle was included as control at a final concentration of 0.5%. After 24–48 h of culture, cell number and viability were measured by adding 20 μL of MTT reagent (5 mg/mL). After 4.5 h of incubation at 37 °C and 5% CO_2, the precipitated formazan crystals were dissolved by adding 100 μL of an acidic sodium dodecyl sulfate solution (10% SDS, 0.01 mol/L HCl) or DMSO. Absorbance was measured at 570 nm. IC_{50} values were calculated with GraphPad Prism software.

2.3. Molecular modeling

The structures of the type 1 chalcones were constructed using the standard tools available in SYBYL 8.0 and the structures were energy-minimized employing the Tripos force field and Gasteiger–Hückel charges. Docking protocols were used as implemented in GOLD 3.1. The X-ray crystal structures of the tubulin-colchicine and tubulin-ABT751 complexes (PDB IDs 1SA0 and 3HKC, respectively) were retrieved from the Protein Data Bank. For the calculations, the ligands were removed and hydrogen atoms were added using the Biopolymer module (SYBYL 8.0). Residues in the binding site were manually checked for possible flipped orientation, protonation and tautomeric states. The binding cavity was centered on the C22 atom of DAMA-colchicine and a radius sphere of 8 Å was considered for the docking procedures, which were repeated 10 times for the *s-cis* and *s-trans* conformations of the type 1 chalcones.

2.4. Inhibition of tubulin assembly

Electrophoretically homogenous bovine brain tubulin (final concentration 10 μM; 1 mg/mL) was pre-incubated with test agents dissolved in DMSO (1% v/v final concentration) and monosodium glutamate (0.8 M final concentration) at 30 °C in 96-well plates. The reaction mixtures were cooled on ice for 10 min and GTP (0.4 mM final concentration) was added. The absorbance at 350 nm was immediately followed in a spectrophotometer. Baselines were established and temperature was quickly raised to 37 °C. The turbidity value after 20 min at 30 °C for 1% DMSO was assigned as 100% assembly, and for colchicine (10 μM) as 0% assembly. The IC_{50} was calculated by nonlinear regression of the percent assembly values at the 20 min time point obtained with 0.625, 1.25, 2.5, 5 and 10 μM test agents.

2.5. Automated high-content cellular analysis

The effects of chalcones **2a**–**2d** and **3a** on mitotic arrest, nuclear morphology and cellular microtubules were studied as previously described [28,29]. HeLa human cervical carcinoma cells (8000/well) were plated in collagen-1-coated 384-well microplates and treated with vehicle (DMSO 0.1% final concentration) or 10 two-fold concentration gradients of test agents within 4–6 h of seeding. Cells were incubated for 18 h at 37 °C and 5% CO_2, fixed with formaldehyde, and labeled with 10 μg/mL Hoechst 33342 in Hank's balanced salt solution (HBSS). Cells were permeabilized with 0.5% (w/w) Triton-X-100 for 5 min at room temperature and incubated with a primary antibody cocktail consisting of an HBSS solution containing rabbit polyclonal antiphosphohistone H3 (Ser10, 1:500, Upstate, Charlottesville, VA, USA), and mouse monoclonal anti-α-tubulin (1:3000, Sigma, St. Louis, MO, USA), followed by a mixture of FITC-labeled donkey anti-mouse IgG (1:500) and Cy3-labeled donkey anti-rabbit IgG (1:500) as secondary cocktail. Cells were rinsed once with HBSS and analyzed with an ArrayScanII high-content reader (Thermo Fisher Cellomics, Pittsburgh, PA, USA) using the Target Activation Bioapplication. Within the application, 1000 individual cells in each well were imaged at three different wavelengths using an Omega XF93 filter set (Omega Optical, Inc., Brattleboro, VT, USA) at excitation/emission wavelengths of 350/461 nm (Hoechst), 494/519 nm (FITC), and 556/573 nm (Cy3). The following parameters were used for data analysis: average nuclear intensity, nuclei per field, average nuclear FITC intensity, and average nuclear Cy3 intensity. A nuclear mask was generated from Hoechst 33342-stained nuclei. MT density and histone H3 phosphorylation were measured in the FITC and Cy3 channel, respectively. MT density was defined as the average green (FITC) pixel intensity in an area defined by the nuclear mask. For determination of mitotic index and nuclear condensation, thresholds for Hoechst 33342 and phosphohistone-H3 intensities were defined as the average Hoechst 33342 or Cy3 intensity plus 1 SD from 28 vehicle-treated wells located in the center of the microplate. Cells were classified as positive if their average Hoechst 33342 or Cy3 intensity exceeded this threshold. EC_{50} values from cell density curves were obtained by a four-parameter logistic equation (GraphPad Prism). The shape of the chromatin condensation, MT density and mitotic index graphs precluded EC_{50} determinations. Accordingly, we determined the minimum detectable effective concentration (MDEC) as an alternative measurement of chalcones and colchicine activities as described previously [38]. To visually illustrate the effects of test agents on cellular MT morphology and mitotic arrest, the identical 384-well plates were then used to acquire higher resolution images of selected wells.

2.6. Cell migration assays

2.6.1. Cell culture

The human breast cancer cell line MDA-MB-231 was kindly provided by Prof. Heloisa Sobreiro Selistre de Araujo (Departamento de Ciências Fisiológicas, Universidade Federal de São Carlos).

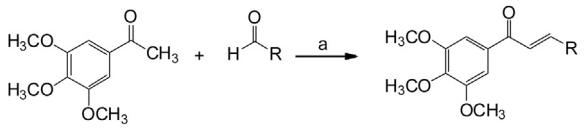

3a R = 4-$N(CH_3)_2$-Ph
3b R = 3,4-Cl_2-Ph
3c R = 4-Cl-Ph
3d R = 4-CH_3-Ph
3e R = 2,6-Cl_2-Ph
3f R = 4-Br-Ph
3g R = 4-NO_2-Ph
3h R = 4-F-Ph
3i R = 4-$O(CH_2)_3CH_3$-Ph
3j R = 3-NO_2-Ph
3k R = 4-OCH_3-Ph
3l R = 2,4,6-triOCH_3-Ph
3m R = 3,4,5-triOCH_3-Ph
3n R = 2,4,5-triOCH_3-Ph
3o R = 3-OCH_3-4-OH-Ph
***3p** R =
***3q** R = 3-CF_3-4-Cl-Ph
3r R = 2,4-Cl_2-Ph
***3s** R = 3,5-Cl_2-Ph

Fig. 3. Preparation of type 2 chalcones. a) KOH 50% w/v, methanol, r.t., 24 h. *Novel compounds, Ph = phenyl.

Table 1
Cancer cell selective cytotoxicity and tubulin polymerization inhibition.

Compound	IC_{50} (μM)						
	L-1210[a]	REH[b]	JURKAT[b]	NIH3T3[a]	HUVEC[a]	PBMC[b]	Tubulin assembly[c]
1a (Colchicine)	ND[d]	0.0095 ± 0.005	0.0077 ± 0.003	0.0026 ± 0.0012	0.023 ± 0.0011	>100	2.3
2a	>100	ND	17.1 ± 1.1	ND	ND	27.0 ± 1.3	>10
2b	54.0 ± 0.5	2.58 ± 0.58	5.90 ± 2.04	ND	ND	35.6 ± 1.1	3.6
2c	26.0 ± 1.0	0.73 ± 0.15	0.50 ± 0.15	34 ± 1.5	37 ± 1.8	18.0 ± 1.2	2.2
2d	47.5 ± 1.5	23.6 ± 1.1	30.0 ± 0.8	ND	ND	81.2 ± 1.1	>10
3a	30.0 ± 0.8	1.05 ± 0.11	1.20 ± 0.15	66 ± 1.4	>100	92.5 ± 1.3	2.8

[a] 24 h MTT assay.
[b] 48 h MTT assay. Data are the averages ± SD of triplicate determinations.
[c] Average of duplicate determinations from a single experiment that was repeated once.
[d] ND, not determined.

The cells were maintained in DMEM (Dulbecco's Modified Eagle's Medium) supplemented with 10% FBS at 37 °C in 5% CO_2 humidified atmosphere. Cell viability was tested by Trypan blue exclusion before experiments.

2.6.2. Wound healing assay

For cell motility determination, cells were seeded in 24-well tissue culture plates (Becton Dickinson) and grown to 80–90% confluence. After aspirating the medium, the centers of the cell monolayers were scraped with a sterile micropipette tip to create a denuded zone. Subsequently, cellular debris was removed by washing with DMEM (without FBS supplementation) and cells were incubated at 37 °C with growth media containing different concentrations of compounds (**1a**, **2c** and **3a**) for 22 h. Pictures of the initial wounded monolayers were taken at 0 and 22 h, and the percentage of wound closure was quantified with ImageJ software.

2.6.3. Boyden chamber migration assay

Cell migration was assayed with Boyden chambers [8.0 μm pore size, polyethylene terephthalate membrane, FALCON cell culture insert (Becton–Dickinson)]. MDA-MB-231 cells were cultured in DMEM until 80–90% confluency. For migration assay, cells were detached with trypsin and resuspended in serum free medium. After cell counting, 4×10^4 cells in serum free media (350 μL) were added to the upper chamber. In the lower chamber, 700 μL of culture medium containing 10% FBS (chemoattractant) were added. The transwells were incubated for 6 h at 37 °C with different concentrations (usually 5–6) of the compounds in both the upper and lower chambers. The control was the vehicle given in the same method. After incubation, cells inside the inserts were removed with a cotton swab and cells on the underside of the insert were fixed with methanol and stained with toluidine blue stain (Sigma). Transmigrated cells were counted with a light microscope, using six random regions of the membrane. The NIS Elements software (NIKON) was used to count the cells. Two independent experiments were carried out in duplicate for each compound.

3. Results and discussion

3.1. Chemistry

The type 1 chalcones **2a**, **2b** and **2c** (Fig. 2) were prepared as previously described [13–15] with yields between 39 and 97%. Chalcone **2d** is a novel compound, obtained by the same methodology as for the other type 1 chalcones, with yield of 94%. The type 2 chalcones (**3a**–**3s**) were prepared by condensation between 3,4,5-trimethoxyacetophenone and corresponding aldehydes (Fig. 3), with yields ranging from 20 to 92%.

All reagents used were available commercially. Synthesized compounds that had been previously reported [7,13–21] were characterized by ^{1}H NMR, ^{13}C NMR and IR (see Supplementary data). Detailed characterization (^{1}H NMR, ^{13}C NMR, IR and elemental analysis) for novel compounds (**2d**, **3p**, **3q** and **3s**) is presented in the Material and Methods section. Previous studies have demonstrated that α-substituted *E*-chalcones may be more potent inhibitors of tubulin polymerization than the corresponding *Z* geometric isomers [6,22]. ^{1}H NMR spectra revealed that, as expected, structures were configured *E* ($J_{H\alpha-H\beta} = \sim 16$ Hz) [6] except for **3a**, which was a 2:1 mixture of *E* ($J_{H\alpha-H\beta} = 16$ Hz) and *Z* ($J_{H\alpha-H\beta} = 12$ Hz) isomers (see Materials and methods Section).

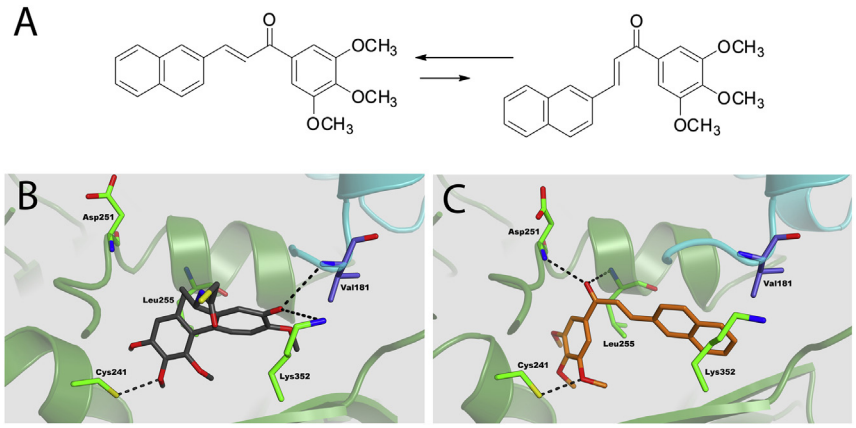

Fig. 4. Molecular modeling studies comparing chalcone 2c with DAMA colchicine. (A) *s-cis* and *s-trans* conformations of **2c**. (B) Crystallographic positioning of DAMA-colchicine (gray) and (C) docking pose of chalcone **2c** (green) in the colchicine binding site. (For interpretation of the references to color in this figure legend, the reader is referred to the web version of this article.)

Table 2
High-content analysis of mitotic arrest in HeLa cells.[a]

Compound	EC_{50} (nM)[b] cell density	MDEC (nM)[b,c]		
		Nuclear condensation	Tubulin intensity	Mitotic index[d]
1a	32.5 ± 4.2	12.0 ± 4.8	10.2 ± 3.8	15.9 ± 2.9
2a	>50,000	>50,000	>50,000	>50,000
2b	3300 ± 600	2200 ± 700	1100 ± 200	1400 ± 100
2c	684 ± 139	317 ± 23	283 ± 52	397 ± 24
2d	>50,000	>50,000	>50,000	>50,000
3a	357 ± 35	217 ± 67	139 ± 13	200 ± 15

[a] 24 h HCS assay.
[b] Average of three independent experiments (±SD).
[c] MDEC, Minimum detectable effective concentration.
[d] Percentage of phospho-histone H3-positive cells.

3.2. Biological evaluation of type 1 chalcones

3.2.1. Mouse leukemia cell growth inhibitory activity

The type 1 chalcones (**2a**–**2d**) were evaluated for their antiproliferative activities against L-1210 murine acute lymphoblastic leukemia cells (Table 1). While the general non-substituted 1,3-diphenylprop-2-en-1-one backbone **2a** was inactive in our tests (**2a,** $IC_{50} > 100$ μM), the addition of a 3,4,5-trimethoxybenzoyl group to the A-ring of the previously characterized 2-naphtaldehyde derivative **2b** resulted in the most potent compound among the type 1 chalcones (**2c**, $IC_{50} = 26$ μM). **2c** showed two-fold improved activity compared with **2b** ($IC_{50} = 54$ μM) [12]. Consistent with findings by Kong et al. [11], the presence of the 2,3,4-trimethoxyphenyl group in the B-ring did not significantly augment cytotoxic potency (**2d**, $IC_{50} = 47.5$ μM).

3.2.2. Molecular modeling studies

Classical ligands of the colchicine site on tubulin (Fig. 1) frequently contain the 3,4,5-trimethoxyphenyl group [6,7,16,23,24], which has been linked to increased antiproliferative potency in type 1 chalcones [6]. This is thought to occur through specific interactions between the trimethoxy groups and colchicine site residues in tubulin, which force the ligand into a curved, *s-trans* conformation. While crystallographic studies suggest that the most probable configuration of chalcones in solution is *s-cis* [25], substitutions at the double bond that force the molecule into an *s-trans* conformation enhance biological activity [6,16]. The crystallographic structure of tubulin complexed with *N*-deacetyl-*N*-(2-mercaptoacetyl)colchicine (DAMA-colchicine, PDB ID 1SA0) was the starting point for docking studies, which were performed to explore possible binding modes for the series of type 1 chalcones at the tubulin α/β intradimer interface. The results suggested that the curved *s-trans* conformer of **2c** overlapped well with DAMA-colchicine within the colchicine binding domain, with their 3,4,5-trimethoxyphenyl groups buried in the same hydrophobic subcavity. The C4-methoxy substituent of **2c** superposed with the C2-methoxy group of colchicine and similarly established a polar interaction with Cys β241 (Fig. 4) [6]. In support of this model, docking of the non-substituted inactive chalcone **2a** did not generate a clearly favored orientation (data not shown). The chalcone–tubulin complex was further stabilized by two hydrogen bonds, involving the carbonyl oxygen of **2c** and the backbone NH of Asp β251 and Leu β255 (Fig. 4). Together, the described intermolecular interactions are consistent with the higher potency observed in compounds having the carbonyl group in a adjacent position to the trimethoxybenzene A-ring, instead of the B-ring as in **2d**.

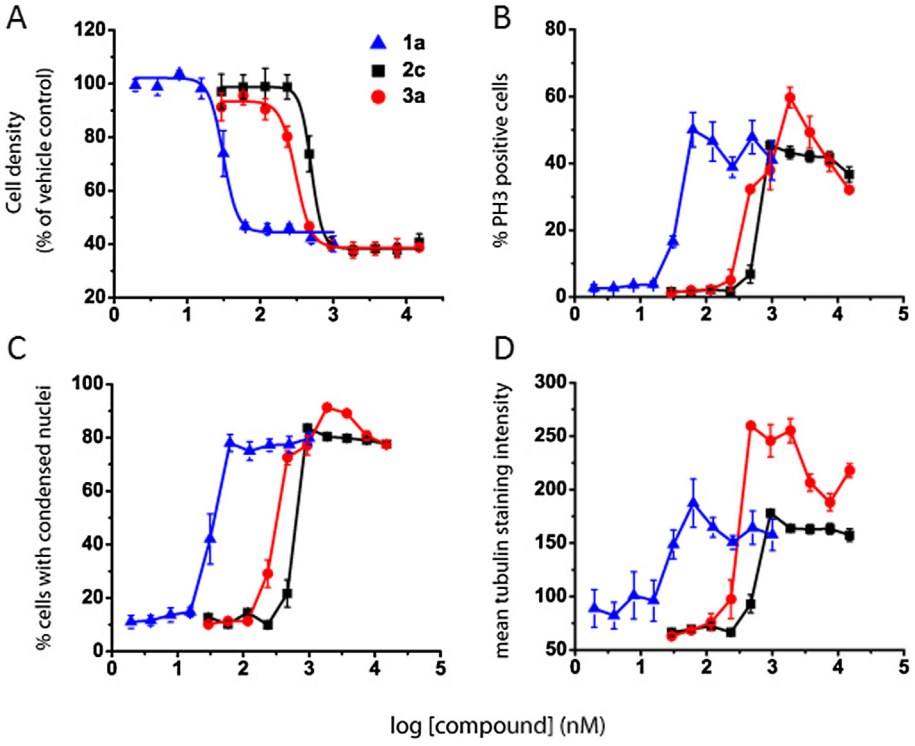

Fig. 5. High-content analysis of mitotic arrest. Cells were treated in 384-well plates with 10 twofold dilutions of colchicine (triangles) and chalcones **2c** (squares) and **3a** (circles), and analyzed by high-content analysis for (A) cell density, (B) Mitotic index, (C) chromatin condensation, and (D) microtubule density. All agents caused cell loss, enhanced mitotic index and nuclear condensation, and provoked an initial increase in microtubule density that plateaued and reversed at higher concentrations. Data are the average ± SEM of quadruplicate wells from a single experiment repeated three times with similar results.

The *s-cis* conformations of the synthesized *E*-chalcones might be more stable than the (more bioactive) *s-trans* conformations [25]. Consistent with this, we observed internal ligand torsion strain penalties for the *s-trans* binding conformations. These penalties were, however, offset by additional van der Waal's interactions contributed by the 2-naphtaldehyde moiety in **2c**, which was positioned at the opposite side of the binding cavity, in the same region as the tropone ring of colchicine [26] (Fig. 4C). Taken together, the data indicate that besides the relative position of the aromatic rings and the carbonyl group, specific substituents on the chalcone moiety are important to correctly anchor the bioactive s-*trans* conformation of chalcone derivatives into the colchicine binding site.

3.2.3. Inhibition of tubulin polymerization

The molecular modeling results suggested that, once bound to the colchicine pocket, cytotoxic type 1 chalcones, like colchicine, could prevent curved tubulin from assuming a straight conformation, thus resulting in cellular MT disassembly and cytotoxic activity [27]. We therefore examined the ability of type 1 chalcones to inhibit tubulin polymerization *in vitro* (Table 1). The 3,4,5-trimethoxyphenyl derivative **2c** had slightly improved ability to inhibit tubulin polymerization compared with the parent **2d,** approaching the potency of colchicine (**1a**). In contrast, the unsubstituted general scaffold **2a** and the 1,3-dioxole derivative **2d** did not inhibit tubulin assembly at concentrations up to 10 μM. Consistent with the tubulin assembly assays, the 3,4,5-trimethoxyphenyl derivative **2c** was more toxic to L-1210 cells than either **2a**, **2b or 2d** (Table 1).

3.3. Biological evaluation of type 2 chalcones

The importance of the 3,4,5-trimethoxy substitution for both inhibition of tubulin assembly and cytotoxic activity encouraged the synthesis of a novel series of type 2 chalcones having the general backbone **3** (Fig. 2).

3.3.1. In vitro cell growth inhibitory activity and inhibition of tubulin polymerization

The type 2 chalcones were first screened for inhibition of cell growth against murine L-1210 cells (see Supplementary data Table S1). Of the nineteen analogs, fourteen (74%) retained antiproliferative activity; the derivative **3a** was the most active ($IC_{50\ (L1210)}$ = 30 μM). Further evaluation in REH and Jurkat human leukemia cells (Table 1) demonstrated that the chalcones **2c** ($IC_{50\ (REH)}$ = 0.73 μM and $IC_{50\ (JURKAT)}$ = 0.50 μM) and **3a** ($IC_{50\ (REH)}$ = 1.05 μM and $IC_{50\ (JURKAT)}$ = 1.20 μM) were at least an order of magnitude more potent against human leukemia cells compared with the murine L-1210 line. **2c** and **3a** also represented a three to twenty five-fold improvement over the type 1 chalcones **2b** ($IC_{50\ (REH)}$ = 2.58 μM and $IC_{50\ (JURKAT)}$ = 5.90 μM) and **2d** ($IC_{50\ (REH)}$ = 23.55 μM and $IC_{50\ (JURKAT)}$ = 30.04 μM). Cytotoxicity

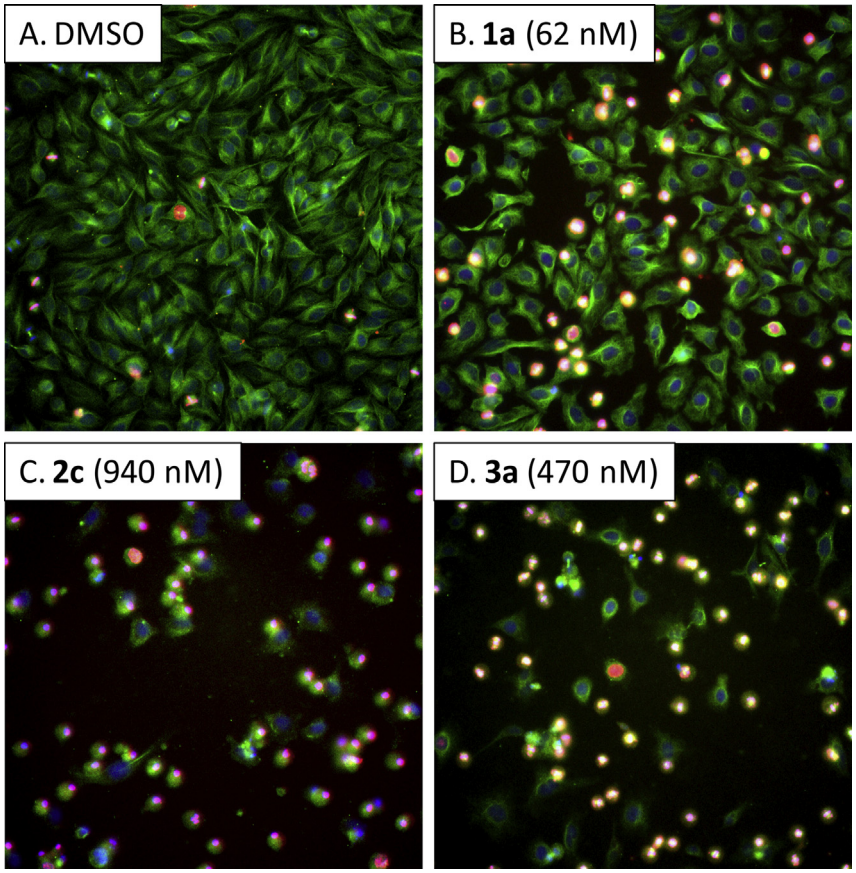

Fig. 6. Mitotic arrest phenotype. HeLa cells were treated with (A) vehicle (dimethyl sulfoxide, DMSO 0.1%), (B) colchicine **1a** (62 nM), (C) **2c**, the most potent type 1 chalcone (940 nM), or (D) **3a**, the most potent type 2 chalcone (470 nM), followed by simultaneous, immunostaining of α-tubulin (green), phosphohistone H3 (red), and Hoechst 33342 (blue). Vehicle-treated cells have highly organized microtubules and a low percentage of mitotic cells. Colchicine **1a** and the chalcones **2c** and **3a** caused a heterogenous response of tubulin disorganization, increased number of phosphohistone H3-positive cells, chromatin condensation, and nuclear fragmentation. Images shown are representative fields from a single experiment repeated three times with similar results. (For interpretation of the references to color in this figure legend, the reader is referred to the web version of this article.)

Table 3
Effect of chalcones **2c** and **3a** on MDA-MB-231 human breast cancer cell migration.

Compound	Scratch assay (% inhibition at 1 μM)[a]	Boyden chamber assay IC_{50} (nM)[b]
1a	74 ± 2	475 ± 106
2c	46 ± 2	1095 ± 29
3a	54 ± 3	656 ± 119

[a] Average ± SD of three independent experiments.
[b] Average ± range of two independent experiments.

evaluations in NIH3T3 immortalized mouse fibroblasts, human umbilical vein endothelial cells (HUVEC), and peripheral blood mononuclear cells (PBMC) revealed that **2c** and **3a** were considerably less toxic to nontransformed cells compared with the two human tumor cell lines (45–100-fold selectivity, Table 1). In contrast, colchicine showed only a 2–3 fold preference for the transformed phenotype, although it was very well tolerated by PBMC (Table 1). Moreover, **3a** (IC_{50} = 2.8 μM) was similar to colchicine **1a** (IC_{50} = 2.3 μM) and compound **2c**, the most potent type 1 chalcone (IC_{50} = 2.2 μM), in its ability to inhibit tubulin assembly *in vitro* (Table 1).

3.3.2. High-content analysis of mitotic arrest

MT-interacting agents typically cause cell cycle arrest and cellular MT perturbations. To investigate the effects of the most potent type 1 and 2 chalcones on cellular MT morphology and mitotic arrest, we conducted our previously described multiparameter high-content analysis [28,29]. We investigated and compared the effects of colchicine **1a**, the type 1 chalcones **2a**–**2d**, and the most potent type 2 chalcone **3a** on MT perturbation, apoptotic morphology, cell cycle arrest and histone H3 phosphorylation. Asynchronously growing HeLa cells were treated for 18 h with each compound or dimethyl sulfoxide (DMSO, 0.1%) as vehicle in collagen-coated 384-well microplates, fixed, and incubated with primary antibodies against tubulin and the mitotic marker protein phosphohistone H3, followed by fluorescein isothiocyanate (FITC) and Cy3-conjugated secondary antibodies, respectively. Cells were detected by nuclear counterstaining with Hoechst 33342, which also provided information about chromatin condensation and cell density as markers of cell death.

Multi-parametric analysis of mitotic arrest showed that like colchicine (**1a**), chalcones **2b**, **2c** and **3a** provoked cell loss, chromatin condensation, and an increase in the percentage cells with elevated phosphohistone H3 levels (Table 2). These same compounds also showed a biphasic response in the measurements of cellular MTs, previously observed for MT-destabilizing agents (Fig. 5) [28,29]. At lower concentrations, tubulin staining intensity increased due to cell rounding and concentration of MTs in a smaller area. At higher concentrations, MT density measurements plateaued and subsequently decreased because of the drug-induced shift of the dynamics of MTs toward tubulin monomers and extraction of monomeric tubulin during the permeabilization process [28]. **2c** and **3a** inhibited attachment and survival of HeLa

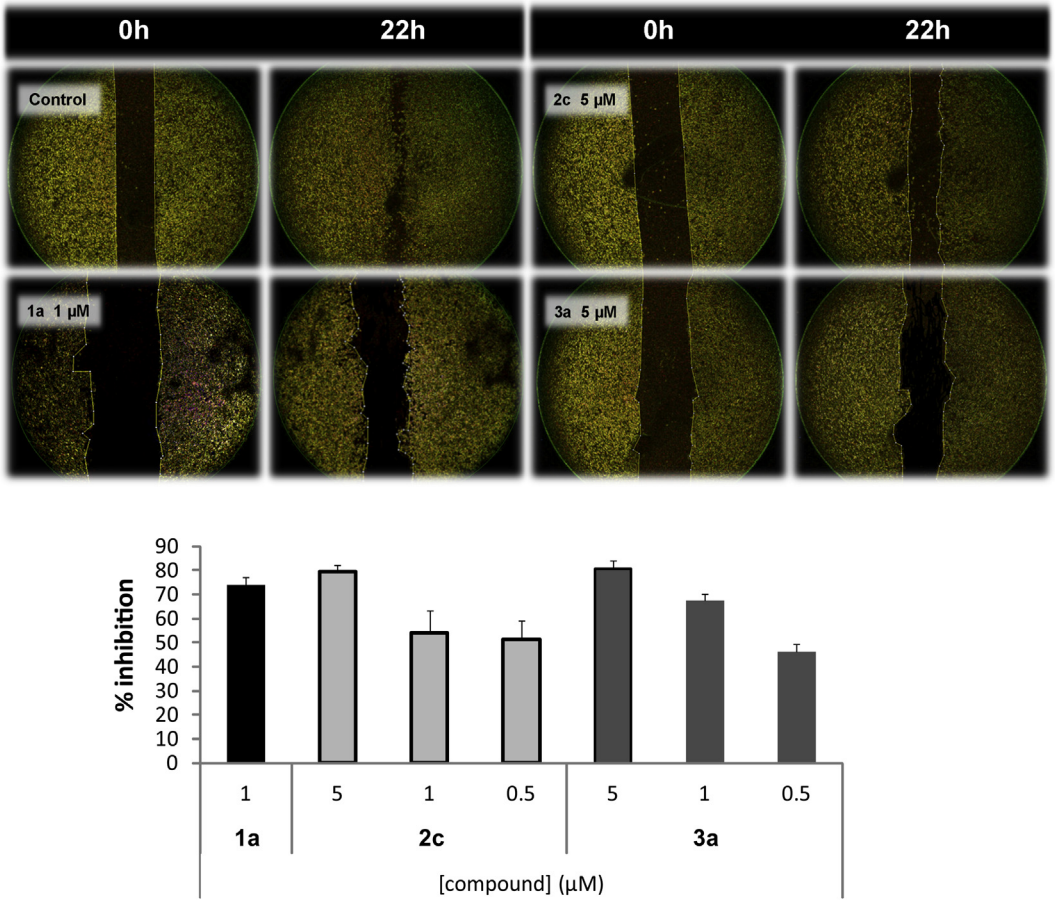

Fig. 7. Inhibition of MDA-MB-231 human breast tumor cell migration in a scratch wound assay. (*Upper panel*) Pictures of wound healing assay at 0 h and 22 h, comparing the wound closure by colchicine **1a** and the chalcones **2c** and **3a**. (*Lower panel*) Quantitative measurements of gap closure inhibition by **2c** and **3a** at three different concentrations. Data are the average ± SEM of triplicate wells from a single experiment repeated twice with similar results.

cells at submicromolar concentrations, representing a five to ten-fold improvement over the parent chalcone **2d,** and a mere ten-fold loss of potency compared with the natural product, colchicine (**1a**) (Fig. 5). Moreover, **2c** and **3a** induced mitotic arrest as measured by chromatin condensation and increasing percentages of cells with elevated phosphohistone H3 as well as perturbed cellular MTs. In contrast, agents that did not inhibit tubulin assembly **(2a** and **2d)** did not cause mitotic arrest in HeLa cells at concentrations up to 50 μM (Table 2). Fluorescence micrographs of representative images of nuclei (blue), tubulin (green), and phosphohistone H3 (red) staining (Fig. 6) confirmed that, while vehicle-treated cells had organized MTs and a low percentage of mitotic cells, cells treated with colchicine showed disorganized MTs and a high percentage of cells with elevated histone H3 phosphorylation levels. High-nanomolar concentrations of **2c** and **3a** caused similar MT disorganization and an increase in the percentage of mitotic cells. Hoechst 33342 counterstaining revealed the presence of condensed and fragmented nuclei characteristic of apoptosis. These results validated the chalcone core structure as a bona fide inhibitor of MT assembly in mammalian cells.

3.3.3. *Effects on cell migration*

Besides their effects on cell division, MT-interacting agents can also interfere with cell migration [30–33]. Directional migration of cancer cells requires changes in cell polarity and remodeling of the cytoskeleton, including the regulation of MTs, actin, and intermediate filaments at the leading edge of the cell. We therefore examined the effects of colchicine **1a**, and the most potent type 1 and 2 chalcones, **2c** and **3a**, on cell migration (Table 3 and Fig. 7). For cellular assays, we selected the MDA-MB-231 human breast cancer cell line, an estrogen independent breast cancer model that we have used previously in cell migration assays because of its high metastatic potential [34]. Initially, chalcones **2c** and **3a** were evaluated at three different concentrations in a scratch wounding assay, which involves the response of confluent monolayer cells to mechanical injury [35]. All three compounds significantly inhibited cell migration in the scratch wound assay (Fig. 7). Based on the results from the wound healing experiments, we performed concentration-dependence experiments in transwell cell culture chambers, which confirmed the antimigratory activities of the two chalcones (Fig. 8). **2c** and **3a** inhibited MDA-MB-231 cell migration in both wound healing and transwell assays with IC_{50} values approaching that of colchicine (Table 3). These results suggest that chalcones **2c** and **3a** should be explored as anti-metastatic agents. Our findings are consistent with studies that demonstrated the ability of combretastatin A-4 to inhibit the migration of bladder cancer cells [36]. In this study, the reduction of cell migration by combretastatin A-4 was attributed in part to decreased AKT protein expression, which is involved with tumor cell survival, proliferation, migration and invasiveness [36]. In this context, our results generate enthusiasm for further investigations of the exact molecular mechanisms of the antimigratory activity of the developed chalcones.

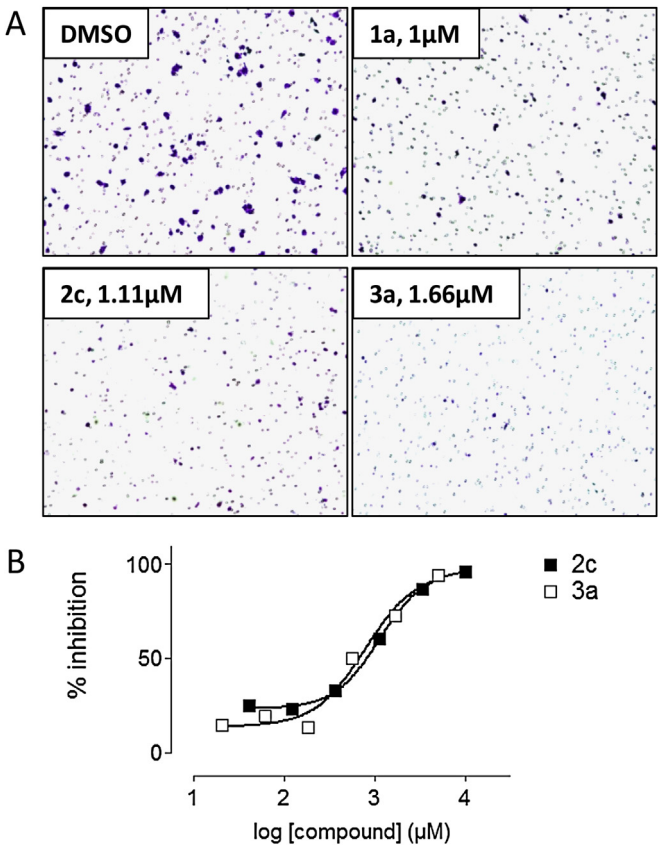

Fig. 8. Effect of chalcones on MDA-MB-231 cell migration using Boyden chamber assays. (A) Representative micrographs of cells that migrated through the membrane insert after staining with toluidine. (B) Quantitation of antimigratory response. Data are from a single experiment that has been repeated once with identical results.

4. Conclusions

We designed, synthesized, and evaluated the biological activities of type 1 and 2 chalcones as potential anticancer agents. The most active agents inhibited tubulin assembly *in vitro* with potencies comparable to colchicine and were only an order of magnitude less potent than colchicine in human cancer cell toxicity assays. The presence of a 3,4,5-trimethoxyphenyl group in ring A appeared beneficial for tubulin interaction, antiproliferative, and antimitotic effects. Our data suggest that the most cytotoxic type 1 and 2 chalcones kill cancer cells by inducing apoptosis and/or mitotic catastrophe through a mechanism that involves MT destabilization. Furthermore, our chalcones showed selective cytotoxicity to cancer cells compared with non-tumorigenic cells and inhibited the motility of a highly metastatic breast cancer cell line in two different types of migration assays. These properties make the 3,4,5-trimethoxyphenyl chalcone pharmacophore an attractive scaffold for further development. We are currently pursuing new analogs of compounds **2c** and **3a** with structural modifications predicted to increase potency, such as restricting the conformation of the double bond to the *s-trans* configuration. Future studies will focus on additional cancer-related activities such as anchorage independent cell growth and invasion, on the elucidation of intracellular signaling pathways that mediate compound toxicity, and on preclinical testing in human tumor xenograft models.

Acknowledgments

We would like to thank CNPq, CAPES and FAPESP for financial support and fellowships. We also thank the Departamento de Química da Universidade Federal de Santa Catarina for equipment used in chemical analysis and the Departamento de Ciências Fisiológicas, Universidade Federal de São Carlos for the cell material. For technical support, we thank Fernanda Spezia Pedrini (Universidade Federal de Santa Catarina) and Laura Lee Vollmer (The University of Pittsburgh Drug Discovery Institute). This project was supported in part by National Institutes of Health grant CA78039, and used the UPCI Chemical Biology Facility that is supported in part by award P30CA047904.

Appendix A. Supplementary data

Supplementary data related to this article can be found at http://dx.doi.org/10.1016/j.ejmech.2013.02.037.

References

[1] M.A. Jordan, L. Wilson, Microtubules as a target for anticancer drugs, Nat. Rev. Cancer 4 (2004) 253–265.
[2] J.A. Hadfield, S. Ducki, N. Hirst, A.T. McGown, Tubulin and microtubules as targets for anticancer drugs, Prog. Cell. Cycle Res. 5 (2003) 309–325.
[3] A. Jordan, J.A. Hadfield, N.J. Lawrence, A.T. McGown, Tubulin as a target for anticancer drugs: agents which interact with the mitotic spindle, Med. Res. Rev. 18 (1998) 259–296.
[4] G.G. Dark, S.A. Hill, V.E. Prise, G.M. Tozer, G.R. Pettit, D.J. Chaplin, Combretastatin a-4, an agent that displays potent and selective toxicity toward tumor vasculature, Cancer Res. 57 (1997) 1829–1834.
[5] G.M. Tozer, C. Kanthou, B.C. Baguley, Disrupting tumour blood vessels, Nat. Rev. Cancer 5 (2005) 423–435.
[6] S. Ducki, Antimitotic chalcones and related compounds as inhibitors of tubulin assembly, Anticancer Agents Med. Chem. 9 (2009) 336–347.
[7] M.L. Edwards, D.M. Stemerick, P.S. Sunkara, Chalcones: a new class of antimitotic agents, J. Med. Chem. 33 (1990) 1948–1954.
[8] S. Tuncel, J. Fournier-dit-Chabert, F. Albrieux, V. Ahsen, S. Ducki, F. Dumoulin, Towards dual photodynamic and antiangiogenic agents: design and synthesis of a phthalocyanine-chalcone conjugate, Org. Biomol. Chem. 10 (2012) 1154–1157.
[9] C. Dyrager, M. Wickstrom, M. Friden-Saxin, A. Friberg, K. Dahlen, E.A. Wallen, J. Gullbo, M. Grotli, K. Luthman, Inhibitors and promoters of tubulin polymerization: synthesis and biological evaluation of chalcones and related dienones as potential anticancer agents, Bioorg. Med. Chem. 19 (2011) 2659–2665.
[10] J. Rodrigues, C. Abramjuk, L. Vasquez, N. Gamboa, J. Dominguez, B. Nitzsche, M. Hopfner, R. Georgieva, H. Baumler, C. Stephan, K. Jung, M. Lein, A. Rabien, New 4-maleamic acid and 4-maleamide peptidyl chalcones as potential multitarget drugs for human prostate cancer, Pharm. Res. 28 (2011) 907–919.
[11] Y. Kong, K. Wang, M.C. Edler, E. Hamel, S.L. Mooberry, M.A. Paige, M.L. Brown, A boronic acid chalcone analog of combretastatin a-4 as a potent antiproliferation agent, Bioorg. Med. Chem. 18 (2010) 971–977.
[12] F.S. Pedrini, L.D. Chiaradia, M.A. Licinio, A.C. de Moraes, J.C. Curta, A. Costa, A. Mascarello, T.B. Creczinsky-Pasa, R.J. Nunes, R.A. Yunes, M.C. Santos-Silva, Induction of apoptosis and cell cycle arrest in l-1210 murine lymphoblastic leukaemia cells by (2e)-3-(2-naphthyl)-1-(3'-methoxy-4'-hydroxy-phenyl)-2-propen-1-one, J. Pharm. Pharmacol. 62 (2010) 1128–1136.
[13] E.H. Alberton, R.G. Damazio, L.H. Cazarolli, L.D. Chiaradia, P.C. Leal, R.J. Nunes, R.A. Yunes, F.R. Silva, Influence of chalcone analogues on serum glucose levels in hyperglycemic rats, Chem. Biol. Interact. 171 (2008) 355–362.
[14] A.L. Navarini, L.D. Chiaradia, A. Mascarello, M. Fritzen, R.J. Nunes, R.A. Yunes, T.B. Creczynski-Pasa, Hydroxychalcones induce apoptosis in b16-f10 melanoma cells via gsh and atp depletion, Eur. J. Med. Chem. 44 (2009) 1630–1637.
[15] L.D. Chiaradia, A. Mascarello, M. Purificacao, J. Vernal, M.N. Cordeiro, M.E. Zenteno, A. Villarino, R.J. Nunes, R.A. Yunes, H. Terenzi, Synthetic chalcones as efficient inhibitors of mycobacterium tuberculosis protein tyrosine phosphatase ptpa, Bioorg. Med. Chem. Lett. 18 (2008) 6227–6230.
[16] S. Ducki, D. Rennison, M. Woo, A. Kendall, J.F. Chabert, A.T. McGown, N.J. Lawrence, Combretastatin-like chalcones as inhibitors of microtubule polymerization. Part 1: synthesis and biological evaluation of antivascular activity, Bioorg. Med. Chem. 17 (2009) 7698–7710.
[17] B.A. Bhat, K.L. Dhar, S.C. Puri, A.K. Saxena, M. Shanmugavel, G.N. Qazi, Synthesis and biological evaluation of chalcones and their derived pyrazoles as potential cytotoxic agents, Bioorg. Med. Chem. Lett. 15 (2005) 3177–3180.
[18] N.J. Lawrence, E.S.M. Armitage, B. Greedy, D. Cook, S. Ducki, A.T. McGown, The synthesis of indanones related to combretastatin a-4 via microwave-assisted nazarov cyclization of chalcones, Tetrahedron Lett. 47 (2006) 1637–1640.
[19] R. Romagnoli, P.G. Baraldi, M.D. Carrion, C.L. Cara, O. Cruz-Lopez, D. Preti, M. Tolomeo, S. Grimaudo, A. Di Cristina, N. Zonta, J. Balzarini, A. Brancale, T. Sarkar, E. Hamel, Design, synthesis, and biological evaluation of thiophene analogues of chalcones, Bioorg. Med. Chem. 16 (2008) 5367–5376.
[20] D. Batovska, S. Parushev, B. Stambohyska, I. Tsvetkova, M. Ninova, H. Najdenski, Examination of growth inhibitory properties of synthetic chalcones for which antibacterial activity was predicted, Eur. J. Med. Chem. 44 (2009) 2211–2218.
[21] Y.K. Rao, S.H. Fang, Y.M. Tzeng, Synthesis and biological evaluation of 3 ',4 ',5 '-trimethoxychalcone analogues as inhibitors of nitric oxide production and tumor cell proliferation, Bioorg. Med. Chem. 17 (2009) 7909–7914.
[22] D.J. Kerr, E. Hamel, M.K. Jung, B.L. Flynn, The concise synthesis of chalcone, indanone and indenone analogues of combretastatin a4, Bioorg. Med. Chem. 15 (2007) 3290–3298.
[23] N.J. Lawrence, R.P. Patterson, L.L. Ooi, D. Cook, S. Ducki, Effects of alpha-substitutions on structure and biological activity of anticancer chalcones, Bioorg. Med. Chem. Lett. 16 (2006) 5844–5848.
[24] R.B. Ravelli, B. Gigant, P.A. Curmi, I. Jourdain, S. Lachkar, A. Sobel, M. Knossow, Insight into tubulin regulation from a complex with colchicine and a stathmin-like domain, Nature 428 (2004) 198–202.
[25] S. Ducki, R. Forrest, J.A. Hadfield, A. Kendall, N.J. Lawrence, A.T. McGown, D. Rennison, Potent antimitotic and cell growth inhibitory properties of substituted chalcones, Bioorg. Med. Chem. Lett. 8 (1998) 1051–1056.
[26] R. Romagnoli, P.G. Baraldi, A. Brancale, A. Ricci, E. Hamel, R. Bortolozzi, G. Basso, G. Viola, Convergent synthesis and biological evaluation of 2-amino-4-(3',4',5'-trimethoxyphenyl)-5-aryl thiazoles as microtubule targeting agents, J. Med. Chem. 54 (2011) 5144–5153.
[27] M. Botta, S. Forli, M. Magnani, F. Manetti, Molecular modeling approaches to study the binding mode on tubulin of microtubule destabilizing and stabilizing agents, Top. Curr. Chem. 286 (2009) 279–328.
[28] A. Vogt, P.A. McPherson, X. Shen, R. Balachandran, G. Zhu, B.S. Raccor, S.G. Nelson, M. Tsang, B.W. Day, High-content analysis of cancer-cell-specific apoptosis and inhibition of in vivo angiogenesis by synthetic (-)-pironetin and analogs, Chem. Biol. Drug Des. 74 (2009) 358–368.
[29] Z. Wang, P.A. McPherson, B.S. Raccor, R. Balachandran, G. Zhu, B.W. Day, A. Vogt, P. Wipf, Structure-activity and high-content imaging analyses of novel tubulysins, Chem. Biol. Drug Des. 70 (2007) 75–86.
[30] G. Yucel, A.E. Oro, Cell migration: Gsk3beta steers the cytoskeleton's tip, Cell 144 (2011) 319–321.
[31] H.L. Yang, A. Ganguly, F. Cabral, Inhibition of cell migration and cell division correlates with distinct effects of microtubule inhibiting drugs, J. Biol. Chem. 285 (2010) 32242–32250.
[32] J.V. Small, B. Geiger, I. Kaverina, A. Bershadsky, How do microtubules guide migrating cells? Nat. Rev. Mol. Cell. Biol. 3 (2002) 957–964.
[33] B. Pourroy, S. Honore, E. Pasquier, V. Bourgarel-Rey, A. Kruczynski, C. Briand, D. Braguer, Antiangiogenic concentrations of vinflunine increase the interphase microtubule dynamics and decrease the motility of endothelial cells, Cancer Res. 66 (2006) 3256–3263.
[34] A. Vogt, K.E. Pestell, B.W. Day, J.S. Lazo, P. Wipf, The antisignaling agent sc-alpha alpha delta 9, 4-(benzyl-(2-[(2,5- diphenyloxazole-4-carbonyl)amino] ethyl)carbamoyl)- 2- decanoylaminobutyric acid, is a structurally unique phospholipid analogue with phospholipase c inhibitory activity, Mol. Cancer Ther. 1 (2002) 885–892.
[35] C.C. Liang, A.Y. Park, J.L. Guan, In vitro scratch assay: a convenient and inexpensive method for analysis of cell migration in vitro, Nat. Protoc. 2 (2007) 329–333.
[36] C.H. Shen, J.J. Shee, J.Y. Wu, Y.W. Lin, J.D. Wu, Y.W. Liu, Combretastatin a-4 inhibits cell growth and metastasis in bladder cancer cells and retards tumour growth in a murine orthotopic bladder tumour model, Br. J. Pharmacol. 160 (2010) 2008–2027.
[37] T. Mosmann, Rapid colorimetric assay for cellular growth and survival: application to proliferation and cytotoxicity assays, J. Immunol. Methods 65 (1983) 55–63.
[38] C. Madiraju, M.C. Edler, E. Hamel, B.S. Raccor, R. Balachandran, G. Zhu, K.A. Giuliano, A. Vogt, Y. Shin, J.H. Fournier, Y. Fukui, A.M. Bruckner, D.P. Curran, B.W. Day, Tubulin assembly, taxoid site binding, and cellular effects of the microtubule-stabilizing agent dictyostatin, Biochemistry 44 (2005) 15053–15063.